ChemistrySelect

Research Article
doi.org/10.1002/slct.202203016

Chemistry Europe
European Chemical Societies Publishing

www.chemistryselect.org

Structural, Spectroscopic Characterization and Application of a Co(II) Coordination Polymer [Co(suc)(bpm)]·$2H_2O$

Luann R. D'souza, Nikita N. Harmalkar, and Sunder N. Dhuri*[a]

A Co(II) coordination polymer [Co(suc)(bpm)]·$2H_2O$ (**1**) built from succinate (suc) and bipyrimidine (bpm) is synthesized hydrothermally and characterized by different methods. It crystallizes in a monoclinic space group $P2_1/n$ with an intriguing 3*D* polymeric architecture. The weak antiferromagnetic (AF) exchange interactions were evinced by Curie Constant (C) = 1.803 $cm^3mol^{-1}K$ and a negative Weiss constant (φ) = −30.163 K. Type VI adsorption isotherm behavior of **1** at 77 K revealed its non-porous property. Compound **1** was investigated and successfully utilized as an additive in lowering the decomposition temperature of ammonium nitrate (AN) based fuels as demonstrated from TG and DSC experiments performed in nitrogen atmosphere.

Introduction

The metal-organic coordination compounds incorporate the features of inorganic metal ions and organic ligands leading to the construction of intriguing structural topologies with potential applications in areas such as magnetism, catalysis, luminescence, chemical sensing, and more. The selection of suitable organic ligands is crucial for generating robust extended high-dimensional coordination frameworks, for instance zeolitic imidazolate frameworks (ZIFs) represent a class of polymeric compounds containing transition metal ions (Fe, Co, Cu, Zn) linked by only imidazolate ligands serving potential applications. Hence, a combination of flexible aliphatic or aromatic carboxylic acids along with nitrogen-containing auxiliary ligands serve as ideal candidates for the rational design of polymeric coordination compounds with merits.[1-15] The carboxylate and nitrogen-based ligands usually mediate significant antiferromagnetic (AF) interactions between the paramagnetic metal ions they bridge, thereby generating interesting magnetic systems. Co(II) is deemed to have a rich diversity in magnetic properties like ferromagnetism, antiferromagnetism (AF), canted-spin ferromagnetism, canted-spin antiferromagnetism, spin crossover and long-range ordering.[16] Taking into consideration these aspects, we have employed succinic acid (H_2suc): a flexible aliphatic dicarboxylate containing two carboxylate groups in 1,4 -positions adopting monodentate and bridging coordination modes and 2,2′-bipyrimidine (bpm): a α-diimine tetradentate ligand.[16] Succinic acid portrays a range of conformational possibilities owing to the torsional flexibility of the carbon chain and the C–O bonds.[17] Lately, we have explored the rich structural diversity of Co(II) succinate coordination polymers appended by pyrazine wherein succinate adopted monodentate as well as bis-monodentate coordination modes to Co(II).[18] Bpm is known to behave as a terminal bidentate ligand bonding with a transition metal in *cis*-fashion or as a bis-bidentate bridging ligand connecting two metal ions, depending upon the M: bpm molar ratios.[19–21] These pre-requisites along with solvothermal reaction conditions foster the transmission of electronic interactions between the metals bridged by these ligands.[18,22–25] There has been a great deal of work committed to the first-row transition metals (Fe, Co, Ni, Zn) bridged by bpm, the M···M separation is usually greater than 5.5 Å making it favourable for AF exchange interactions.[1,2,18,22,23,26–31] With the surge in employing solid propellants for use in space and military operations, the propellants comprise the oxidizer (perchlorates or nitrates) and polymeric fuels. The propellants based on ammonium perchlorate (AP) release halogenated emissions which are threatening to life and the environment. Hence, ammonium nitrate (AN) is a potential halogen-free replacement that on blending with metal salts or acids was efficient in lowering the temperature and accelerating the decomposition of AN.[32–38] Hence, our work emphasizes on designing a cobalt(II) coordination polymer by exploiting the excellent coordination abilities of succinic acid and bpm as ligands to yield [Co(suc)(bpm)]·$2H_2O$ (**1**). A thorough characterization of **1** including X-ray crystal structure determination revealed its intriguing polymeric architecture. In addition to this, the magnetic exchange interactions and the role of **1** in inducing the decomposition of AN were also investigated in this paper.

Results and discussion

Synthesis of [Co(suc)(bpm)]·$2H_2O$ (1)

The synthesis was carried out under hydrothermal conditions in a closed vessel under autogenous pressure. The compositional (solvent, pH of reaction mixture, molar ratio of reactants, concentration, counter ions) and process parameters (pressure, temperature, time) possess a profound effect on the assembly of the ligands with the metal centre to generate the overall

[a] *M.Sc. L. R. D'souza, M.Sc. N. N. Harmalkar, Prof. Dr. S. N. Dhuri*
School of Chemical Sciences, Goa University, Taleigao Plateau, Goa, 403 206 India
E-mail: sndhuri@unigoa.ac.in
Homepage: https://www.unigoa.ac.in/faculty/sunder-n-dhuri.html

Supporting information for this article is available on the WWW under https://doi.org/10.1002/slct.202203016

structure.[25] Thus, hydrothermal conditions enhance the solubility of reactants yielding crystals suitable for structural characterization. Hence, it was quite an efficient approach keeping in mind these parameters to get the desired product as already reported in our previous work on synthesizing Co(II)-phenylenediacrylates, succinates and nitro-isophthalates appended by N-donor ligands.[18,39,40]

Table 1. Crystal data and structure refinement for **1**.

Empirical formula	$C_{12}H_{14}CoN_4O_6$
Formula weight (g mol^{-1})	369.19
Temperature (K)	100(2)
Wavelength (Å)	0.71073
Crystal system	Monoclinic
Space group	$P2_1/n$
a (Å)	10.0230(6)
b(Å)	14.1117(9)
c (Å)	10.1074(6)
α (°)	90
β (°)	96.047(2)
γ (°)	90
Volume (Å^3)	1421.65(15)
Z	4
Calc. Density (mg/m^3)	1.725
Absorption coefficient (mm^{-1})	1.246
F(000)	756
Theta range for data collection (°)	2.722 to 28.286
Completeness to theta	99.8
Index ranges	$-12 \le h \le 13$, $-18 \le k \le 18$, $-13 \le l \le 13$
Reflections collected	12691
Independent reflections	3512 (R_{int} = 0.0297)
Refinement method	Full-matrix least-squares on F^2
Absorption correction	None
Data/restraints/parameters	3512/0/224
Goodness-of-fit on F^2	0.952
Final *R* indices [I > 2sigma(I)]	R_1 = 0.0281, wR_2 = 0.0654
*R*indices (all data)	R_1 = 0.0340, wR_2 = 0.0688
Largest diff. peak &hole (e.Å^{-3})	0.607, −0.407
CCDC Number	2179421

Structure Determination of 1

Compound**1** crystallized in the monoclinic $P2_1/n$ space group (Table 1). The asymmetric unit is built from one independent Co(II) ion, two bpm ligands, two suc^{2-}ligands and two crystallization water molecules (Figure 1). Each Co(II) ion coordinates to four nitrogen atoms (N1, N2, N3, N4^{ii}) from two bpm ligands, two oxygen atoms (O1, O4^{iii}) from two suc^{2-}completing the CoN_4O_2 distorted octahedral geometry along with two crystallization water molecules (O1w, O2w). The typical Co–N and Co–O bond lengths lie at 2.1512(14) Å and 2.0299(12) Å respectively as shown in Table S1. This is a consequence of the reduced bite angle of the bpm ligand (76.83° for N1–Co1–N2^{i} and 77.89° for N3–Co1–N4^{ii}) with bpm adopting the bidentate mode (*Mode I*) when linking a single cobalt atom and the bis-bidentate coordination mode (*Mode II*) linking two cobalt atoms through its nitrogen atoms (Co1–N1 and Co1–N2^{i}). The aforementioned binding modes adopted by bpm in **1** are depicted in Figure 2.[1,2,20–23,27,29–31] Both succinate and bpm act as bridging ligands toCo(II) centres with succinate adopting monodentate bridging coordination toCo(II)[18] and bpm exhibiting the bis-bidentate bridging mode, thus forming an array of chains (Figure 3). On account of the bis-bidentate

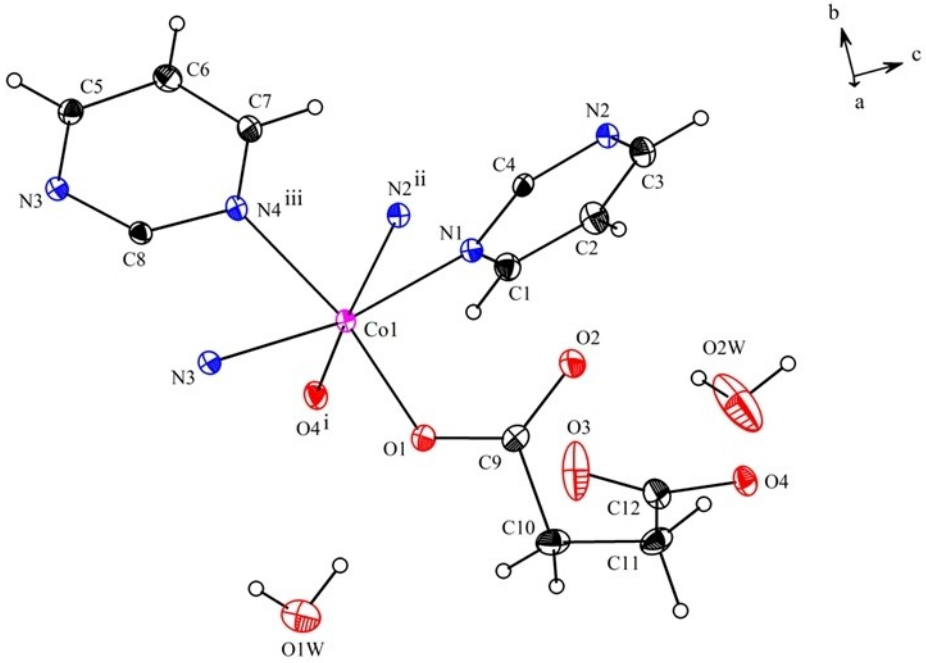

Figure 1. Crystal structure of [Co(suc)(bpm)]·2H_2O(**1**) shows the thermal ellipsoids drawn at the 50% probability level for all of the atoms except for the H atoms that are shown as spheres of arbitrary radii. Symmetry codes: (i) x−1/2, −y+3/2,z+1/2 (ii) -x+1,−y+1,−z+1 (iii) −x+1, −y+1, -z+2.

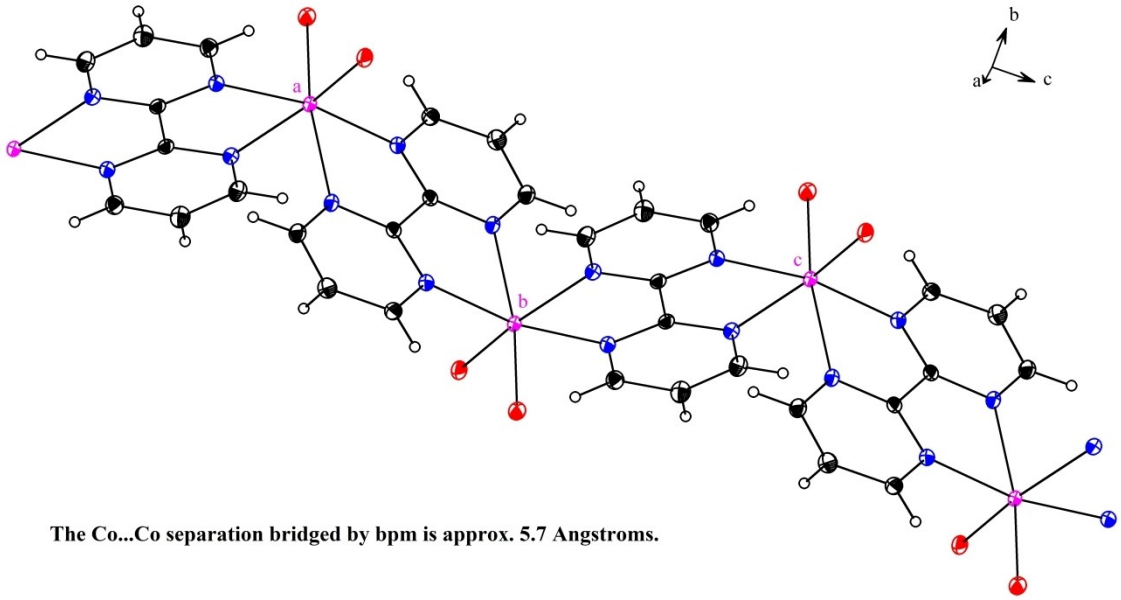

Figure 2. The view of **1** along *a* axis showing the extension of cobalt units through bpm with Co(a)···Co(b) separation of 5.703(2) Å [−x+1, −y+1, −z+1] and Co(b)···Co(c) separation of 5.720(2)Å[−x+1, −y+1, −z+2].

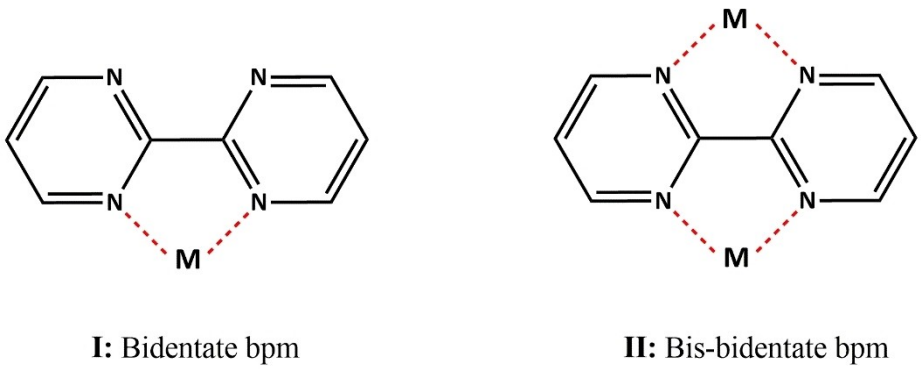

Figure 3. The observed binding modes of bpm in **1**.

chelation mode of bpm, the interchain Co···Co separation across bpm is found to be 5.720(3) Å while that for the succinate bridging theCo(II) centres it is 8.792(6) Å, as can be depicted by Figure 4&Figure S1, lying in accordance with bridging bpmCo(II) compounds reported in the literature (Table S2).[2,19,20–23,26–30,36] The bpm bridges the Co(II) centres extending along one dimension and thereby extending through the other dimension *via* the succinate ligand to generate a *3D* network arrangement with the crystallization water molecules occupying the interstices (Figure S2). On the other hand, an important aspect concerning the succinate ligand bridging the Co(II) centres is the conformational change of *E* and *Z*-forms observed for succinate as shown in Figure S3. The perspective view of **1** along the *c*- axis gives rise to a flower- like supramolecular architecture and the crystallization water molecules present in the interstices give rise to hydrogen bonding interactions with the succinate (Figure S4-S6, Table S3).

Infrared (IR) spectroscopy

The IR spectroscopy is a versatile tool for detection of functional groups. IR was employed to understand the carboxylate and hydrate binding features along with the rigid bpm linker. The IR spectrum of **1** compared with that of succinic acid and bpm shows features attributed to the composition of the coordination polymer. The strong and broad absorptions centred at 3300 cm^{-1}(O–H stretching vibrations) is due to the lattice water molecules. Medium-to-weak absorptions observed between 2890–3040 cm^{-1} are characteristic of C–H stretching vibrations of the organic ligands. The occurrence of strong absorption at 1550 cm^{-1}(ring stretching modes of bpm) is diagnostic of the *bis*-chelating coordination

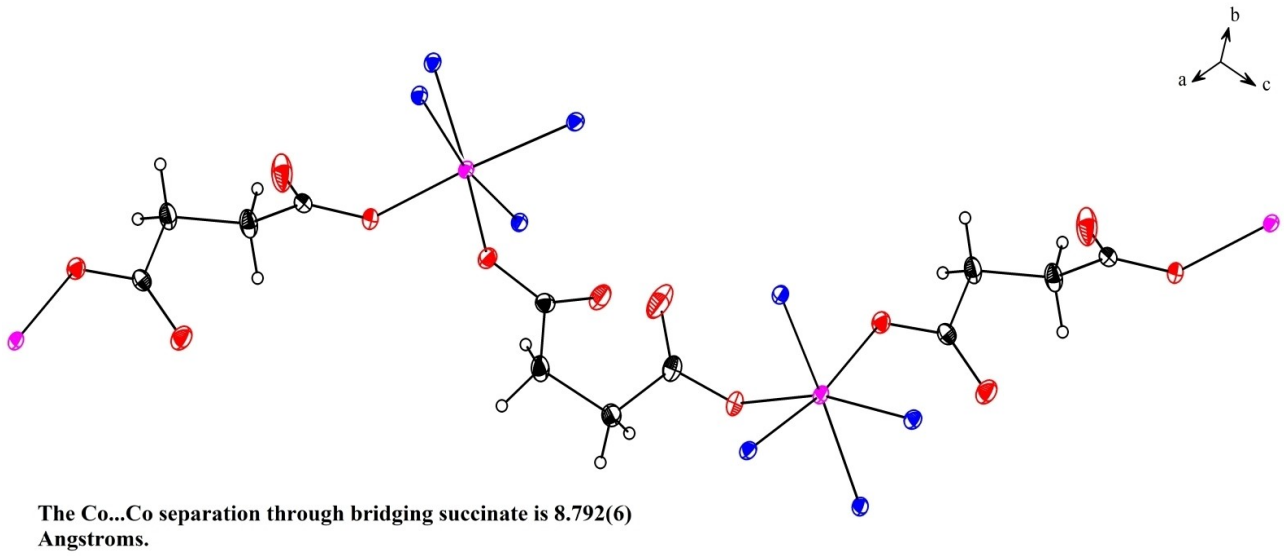

Figure 4. The view of **1** along the *ac* plane shows the extension of cobalt units through succinate with Co1···Co1 separation of 8.792(6) Å [x + 1/2, −y + 3/2, z−1/2].

mode of bpm which is in agreement with the crystal structure data (*vide supra*). The strong-to-medium absorptions between 1460-1400 $cm^{-1}$are attributed to the stretching vibrations of succinate (Figure S7).[2,19,23,26,31]

Thermal Investigation of 1

The thermal profile of **1** is depicted with thermogravimetric (TG), differential thermal analysis (DTA) and derivative thermogravimetric (DTG) measurements performed between 30-650 °C under air atmosphere. The first weight loss step in the TG lies between 35-115 °C accounting for 10.01 % (*calcd.*9.75 %) attributed to two lattice water molecules. This process is evidenced by a small endotherm at 106 °C and 91 °C in the DTA and DTG patterns respectively. Upon dehydration, further heating till 450 °C results in mass loss of 73 % (*calcd.* 74.3 %) due to ligand decomposition evinced by a sharp exo at 428 °C (DTA) and sharp endo at 403 °C (DTG) (Figure 5). The residue of 16.6 % was obtained due to the formation of CoO.

Gas adsorption property

The thermal analysis of **1** revealed loss of two crystallization water molecules at 115 °C followed by robust stability of the dehydrated form up to 310 °C. Moreover, the crystal structural analysis revealed the presence of minute pores as visualised from Mercury 4.2 software (*vide infra*). Hence, this could bethe basis for the robust architecture of **1** serving as a trap for selective gas adsorption. In order to calculate the solvent accessible void in **1**, we used the PLATON software to squeeze the two lattice water molecules. The total potential solvent area volume was calculated to be 136.8 $Å^3$ which accounted for 9.6 % of the unit cell volume of **1**. Hence, we investigated the nitrogen adsorption property of **1** which was degassed at 100 °C for 2 h to ensure removal of adsorbed moisture. The reversible N_2 sorption profile for **1** at 77 K (Figure 6) demonstrated a type VI adsorption isotherm behaviour which describes the typical layer-by-layer adsorption on a uniform non-porous surface with negligible gas uptake and surface area of 0.946 $m^2 g^{-1}$.[41–47]

X-ray powder diffraction pattern of 1

On account of the crystal structure of **1** showing the bpm bridging the Co(II) centres extending along one dimension and thereby extending through the other dimension *via* the succinate ligand to generate a 3D network arrangement with the crystallization water molecules occupying the interstices. To investigate the magnetic behaviour of **1** and employ it as an additive in ammonium nitrate-based fuels, we determined the phase purity of **1** by recording its X-ray powder pattern oand compared it with the simulated X-ray powder patternobtained from the crystal structure (Figure S8).[3]

Field Emission Scanning Electron Microscopy (FESEM) imaging of 1

We evaluated the morphology of **1** by FESEM imaging at different magnifications. The images were found to display cylindrical rods with agglomeration as depicted in Figure 7.

Magnetic property of 1

We investigated the magnetic property of the powdered sample of **1** by temperature-dependent magnetic susceptibility (χ_M) measurements under an applied magnetic field of 1000 G between 10-300 K. From the plot of χ_M*vs* T depicting the Zero Field Cooled-Field Cooled (ZFC-FC) curves, the χ_M values were

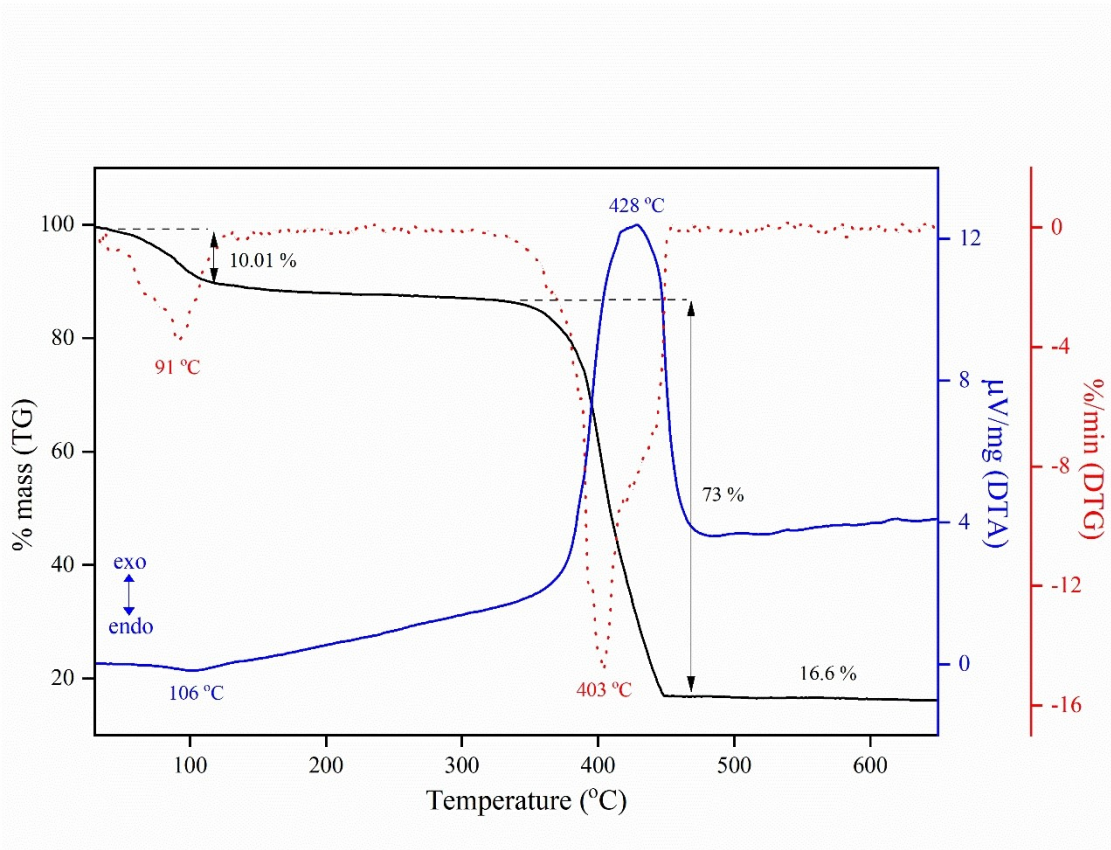

Figure 5. The thermal profile of **1** was depicted by the TG-DTA-DTG plots recorded in the air between 30-650 °C at a heating rate of 10 °C min^{-1}.

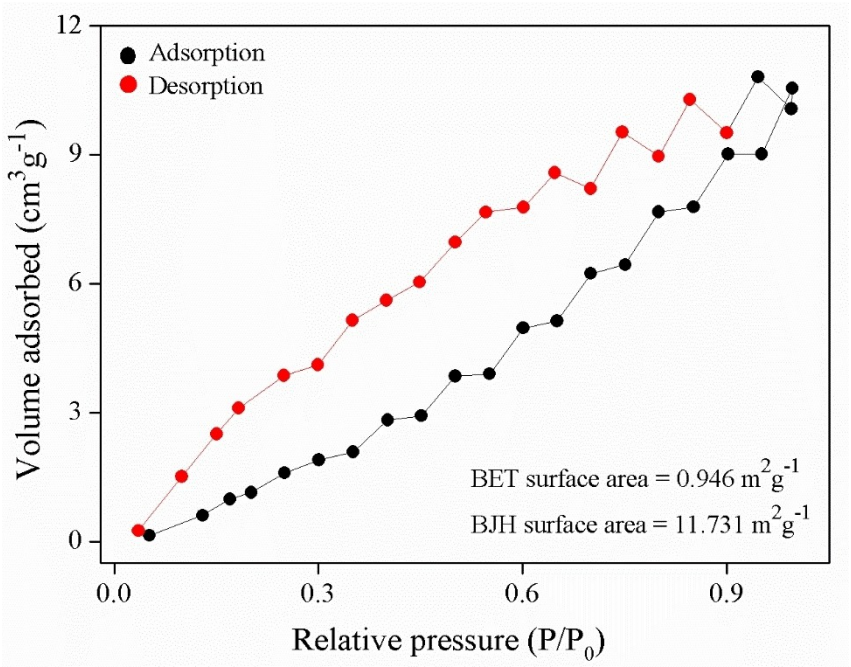

Figure 6. Nitrogen adsorption/desorption isotherms at 77 K for **1**; black spheres, adsorption; red spheres, desorption.

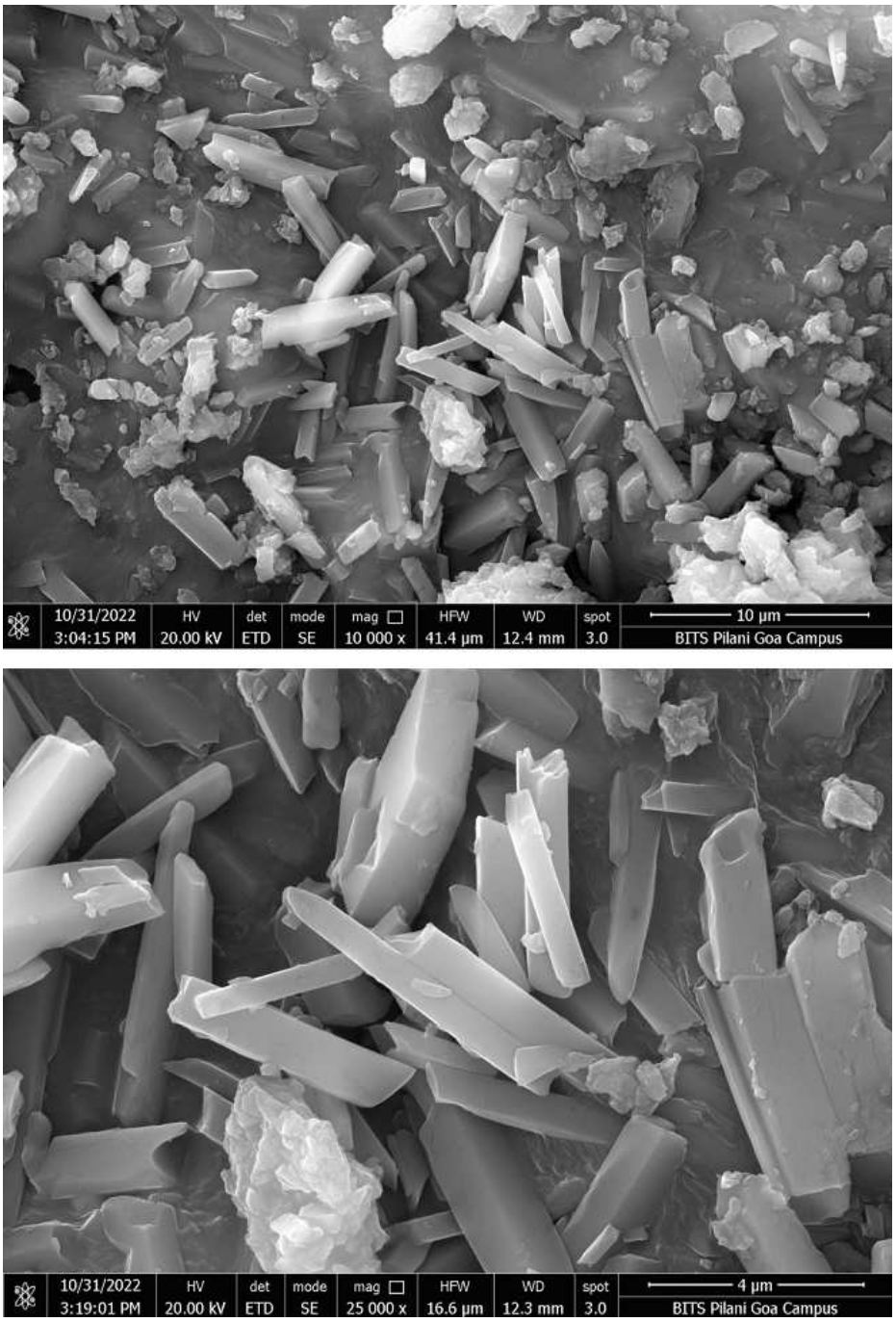

Figure 7. The FESEM images of **1** recorded at magnification scales of 10000X (top) and 25000X(bottom).

found to increaseon lowering the temperature with the curves showing minimum bifurcation suggestive of magnetic ordering. The effective magnetic moment was 4.017 BM calculated using $\mu_{eff} = 2.82(\chi_M T)^{1/2}$, which was slightly higher compared to the calculated spin-only magnetic moment ($\mu_{so} = 3.873$ BM) for high spin Co(II) $3d^7$ system with$S = 3/2$ due to spin-orbit coupling(Figure 8a).[16,18,39] Moreover, $\chi_M T$*vs* T presented a continuous decrease of $\chi_M T$ values upon cooling to 10 K (Figure 8b). This feature is present in Co(II) compounds showing antiferromagnetic interactions among the Co(II) centres mediated through bridging ligands. The crystal structure analysis (*vide infra*) of **1** shows Co(II) centres with average Co···Co distances of 5.720 Å and 8.792 Å flanked by bridging bpm and succinate respectively, sufficiently good for magnetic interactions to occur. These arise from the fact that single- ion anisotropy and antiferromagnetic (AF) interactions are mediated through ligands bridging the Co(II) centres. The plot of $1/\chi_M$*vs* T showed linearity over the entire temperature range obeying the Curie-Weiss law given as; $\chi_M = \frac{C}{T-\phi}$where χ_M is the magnetic susceptibility in $cm^3\ mol^{-1}$, C is the Curie constant in

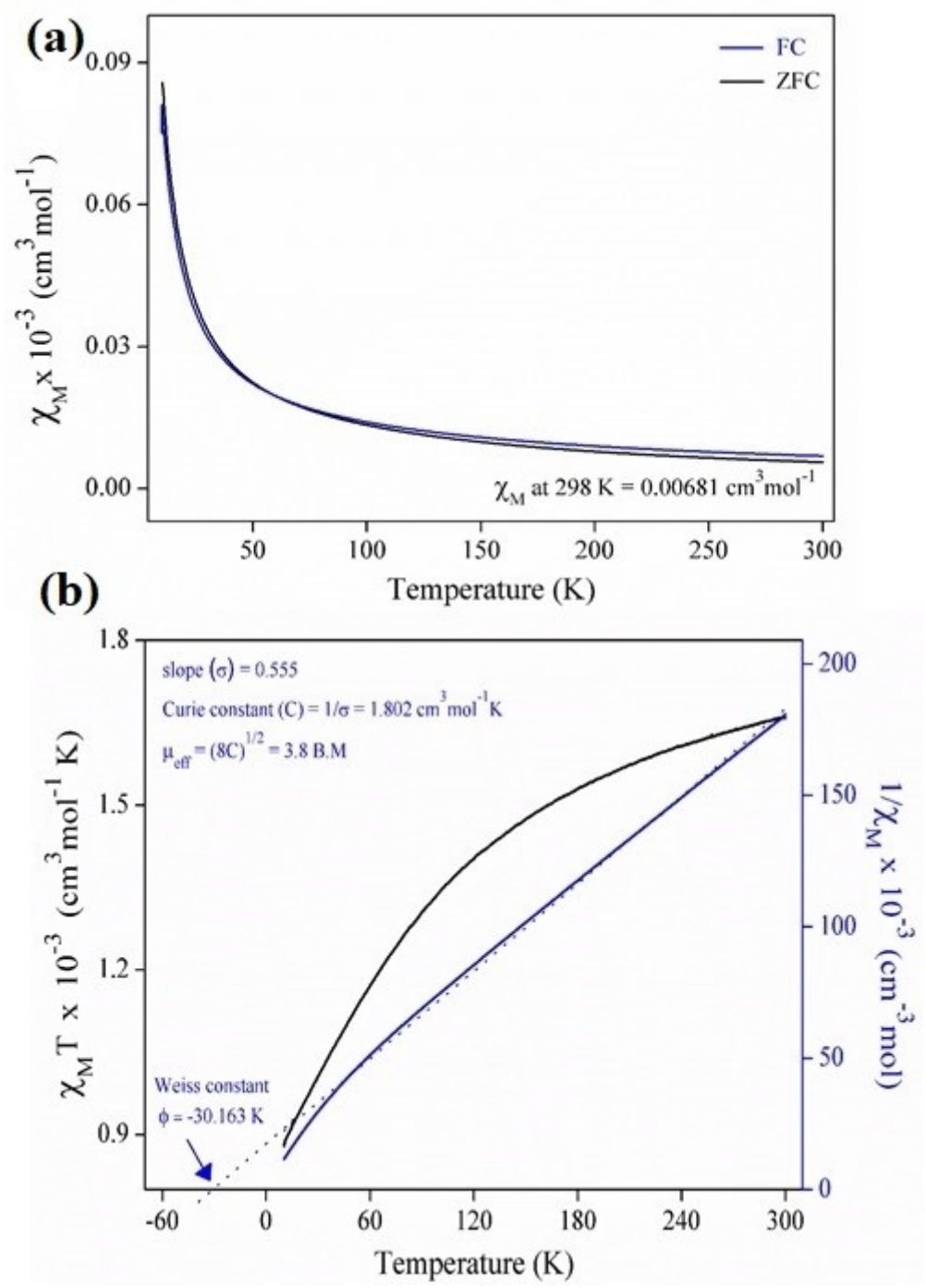

Figure 8. a) The plot of Zero Field Cooled (ZFC)-Field Cooled (FC) magnetic susceptibility for **1** as a function of temperature under an applied field of 1000 G between 10 to 300 K.b) Temperature dependence of $\chi_M T$ and $1/\chi_M$ for **1** under an applied field of 1000 G between 10-300 K. The solid blue line is the theoretical fit to the Curie-Weiss law.

cm^3 $mol^{-1}K$, T is the temperature in Kelvin and φ is the Weiss constant in Kelvin. A fitting of the Curie- Weiss law on the data gave Curie Constant (C) = 1.803 cm^3 mol^{-1} K obtained from inverse of the slope and a negative Weiss constant (φ) = −30.163 K, suggesting weak antiferromagnetic (AF) exchange interactions, evinced from declining $\chi_M T$ values upon cooling with an effective magnetic moment of 3.8 BM using $\mu_{eff} = (8\ C)^{1/2}$.[1,3,18,21,22,26–29,32,33]

Employing 1 as an additive in the decomposition of ammonium nitrate (AN)

We evaluated the thermal characteristics of AN with **1** by performing thermo gravimetric analysis (TGA)-Differential Thermal analysis (DTA)-Derivative Thermal analysis (DTG) and Differential Scanning Calorimetric (DSC) studies by heating the sample between 35-400 °C in a nitrogen atmosphere at 5 °C min^{-1} while DSC experiments were conducted on Perkin Elmer DSC 8000 between 50-400 °C in a nitrogen atmosphere at 2 °C min^{-1}.

From the thermal decomposition profile of neat AN (Figure 9a), AN start disintegrating at ~200 °C and thereafter undergoes complete decomposition at 276 °C evidenced by a sharp endothermic peak at 276 °C in the DTA and DTG patterns. The thermal behaviour of AN/**1** (20 wt%) (Figure 9b) showed complete decomposition at 248 °C indicated by exothermic and endothermic peaks in the DTA and DTG patterns. Hence, this revealed that the burning rate of AN/**1** (20 wt%) as an additive deteriorated faster than the additive-free one (neat AN) with decomposition at 276 °C and 248 °C respectively. Thus, AN/**1** (20 wt%) burnt 28 °C lower than that of neat AN, the

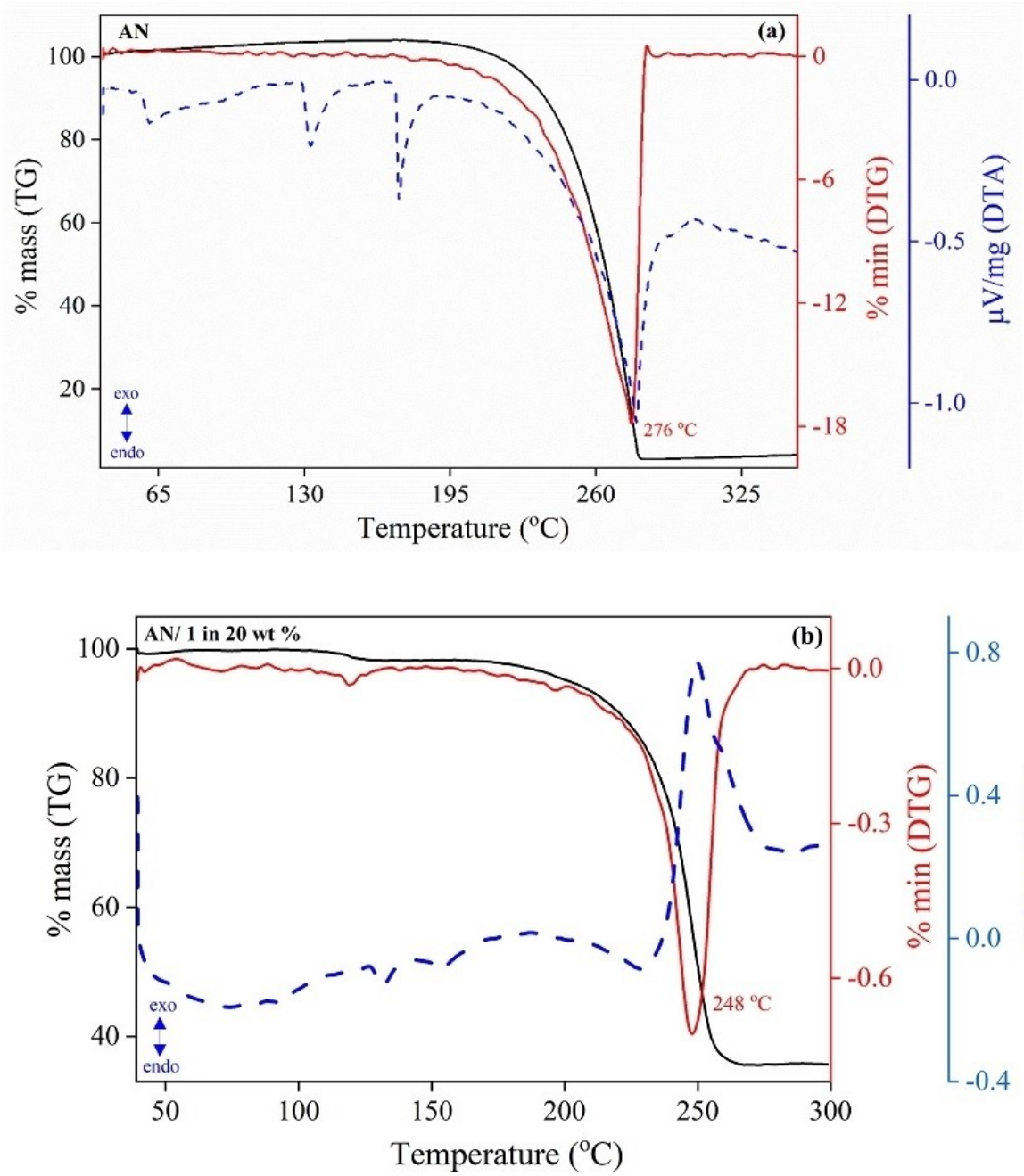

Figure 9. The TG-DTA-DTG plots of (a) neat AN and (b) AN/**1** in 20 wt % were carried out between 35-400 °C at a heating rate of 5 °C min^{-1} in nitrogen atmosphere.

comparative decomposition values for various compounds chosen as an additive in AN decomposition are shown in Table 2.

Moreover, the DSC traces of AN and AN/**1** in 20% wt also revealed similar observations. The DSC traces of neat AN and AN with **1** heated between 50-400 °C at a heating rate of 2 °C min^{-1} in a nitrogen atmosphere are shown in Figure 10. The DSC of neat AN displayed four distinct endothermic peaks at ~50 °C, and ~120 °C attributed to the phase transitions of AN while that at 169 °C indicated the melting point of AN. The large endothermic event at ~276 °C, represented the thermal decomposition of AN. On comparing the decomposition behaviour of a mixture of AN and **1**, we observed only three distinct peaks, at ~50 °C and ~120 °C due to phase transitions with the melting point of AN poorly defined followed by a sharp endothermic peak at 248 °C due to AN decomposition. Hence, these results corroborated with the thermal studies asserting the potential of **1** as an additive in AN-based fuels with less heat evolution.[34–37]

Table 2. An overview of the compounds used as additive with AN.

Sr. No.	Compound	Decomposition of AN (°C)	Reference
1	AN/Nano triaminoguanidine nitrate	252	[35]
2	AN/NaCl	264	[36]
	AN/NH_4Cl	256	
	AN/KCl	256	
	AN/$CaCl_2$	266	
3	AN/Basic Cu(II) nitrate	260	[37]
4	Neat AN	276	Our work
5	AN/**1** in 20 wt %	248	Our work

Conclusions

A new coordination polymer, [Co(suc)(bpm)]·$2H_2O$ (**1**) has been synthesised and characterized by several techniques. The crystal structure of **1** exhibits a flower- like supramolecular network. The bridging succinate and bpm mediatesmagnetic exchange interactions between the Co(II) centres with weak antiferromagnetic exchange interactions. Compound **1** demonstrated a type VI nitrogen adsorption isotherm and was an efficient additive in lowering the exothermic decomposition of AN.

Experimental section

Materials and analysis

All chemicals and solvents were commercially available and used without further purification. The disodium salt of succinic acid (Na_2suc) was prepared by the slow addition of $NaHCO_3$ to the hot aqueous solution of succinic acid (2:1), followed by slow evaporation to give white crystalline flakes. The composition of Na_2suc was studied by IR spectroscopy and elemental analysis (C, H, & N). The necessary safety measures were taken during autoclave syntheses using Teflon-lined stainless steel vessels heated in a temperature-controlled oven (ANTS). The IR spectrum of the powdered compound was recorded on dilution with KBr on Shimadzu (IR Prestige-21) FT-IR spectrometer in the region 4000-350 cm^{-1}at a resolution of 4 cm^{-1}. Elemental analyses (C, H & N) were performed on ElementarVariomicro Cube CHNS Analyzer. The variable-temperature magnetic susceptibility data were obtained on a Vibrating Sample Magnetometer with the sensitivity of a SQUID (Superconducting Quantum Interference Device) of model Quantum Design, MPMS-3 operated between 10-300 K with an applied field of 1000 G. Thermogravimetric analysis accompanied

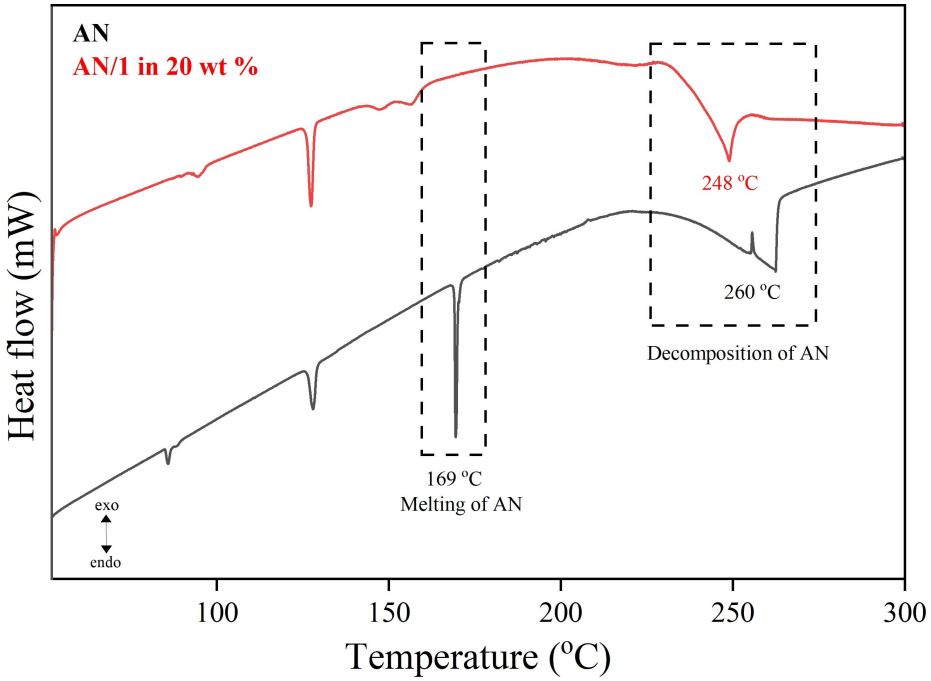

Figure 10. The DSC traces of AN and AN/**1** in 20 wt % were carried out between 50-400 °C at a heating rate of 2 °C min^{-1} in nitrogen atmosphere.

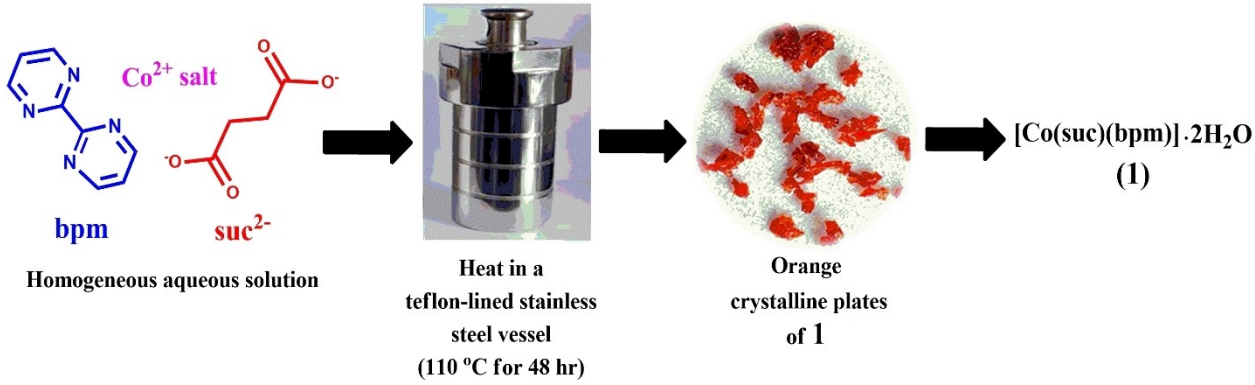

Scheme 1. Synthetic methodology for compound **1**.

by Differential thermal analysis (DTA) and Derivative thermal gravimetry (DTG) were carried out on Netzsch STA 409 analyzer under air atmosphere from RT to 650 °C at a heating rate of 10 °C min^{-1}. Differential scanning calorimetry (DSC) was performed on Perkin Elmer DSC 8000 analyzer under a nitrogen atmosphere from 50-650 °C at a heating rate of 2 °C min^{-1}. X-ray powder diffraction (PXRD) patterns were collected on a RIGAKU ULTIMA IV diffractometer using Cu–Kα (λ = 1.5418 Å) with a Ni filter. The ambient pressure volumetric N_2 adsorption- desorption measurements were performed at77 K maintained by low-temperature liquid nitrogen assembly. The sample was outgassed at 100 °C for 2 h. The adsorption data in the pressure range < 0.1 P/P_o were fitted to the Brunauer-Emmett-Teller (BET) equation to determine the surface area. The Field Emission Scanning Electron Microscope (FESEM) imaging was done on Quanta FEG 250 at 20 KV with a magnification ranging 10000X–25000X.

Single crystal X-ray diffraction

The single crystals of **1** were structurally analyzed on a Bruker D8 Quest Eco model X-ray diffractometer equipped with Mo-(Kα) = 0.71073 Å radiation at 100 K. The X-ray diffraction intensities were collected, integrated, and scaled and unit cell parameters were determined using the program suite APEX3 (Version 2018.1). The structure was solved by direct methods with SHELXS and subsequent refinements on F^2 using full-matrix least-squares methods were performed with SHELXL7.[48] The non-hydrogen atoms were refined with the anisotropic displacement parameters while the hydrogen atoms were located at the calculated positions.

Synthesis of [Co(suc)(bpm)]·$2H_2O$ (1)

An aqueous solution (2 mL) of $Co(NO_3)_2 6H_2O$ (1 mmol, 0.291 g) was added dropwise to an aqueous mixture (3 mL) of disodium succinate (1 mmol, 0.162 g) and bpm (3 mmol, 0.474 g). The resulting orange solution was stirred at room temperature (RT) for 5 mins and then transferred into a 10 mL Teflon-lined stainless steel autoclave which was heated at 110 °C for 48 hours under autogenous pressure (Scheme 1). Orange plate-like crystals of **1** were obtained, separated and dried in air (Yield = 0.055 g).*Anal. Calc.* for **1** $C_{12}H_{14}N_4O_6Co$ (Mr. = 369.2): C, 39.04; H, 3.82; N, 15.18. *Found*: C, 38.55; H, 3.75; N, 15.01. *IR (KBr*,cm^{-1}): 3680 (w), 3300 (br), 3033 (w), 2327 (w), 1970 (w), 1765 (w), 1560 (s), 1424 (s), 1245 (s), 1155 (s), 1117 (s), 1040 (s), 937 (s), 900 (s), 835 (s), 758 (s), 670 (s), 502 (s), 464 (s).

CCDC: Deposition Number 2179421, contain the supplementary crystallographic data for this paper. These data are provided free of charge by the joint Cambridge Crystallographic Data Centre and Fachinformationszentrum Karlsruhe Access Structures service.

Acknowledgements

SND and LRD gratefully acknowledge financial support from CSIR (Grant No. 01(2923)/18/EMR-II). The authors acknowledge IISER Bhopal for assisting with the SQUID-VSM facility and BITS Pilani Goa for FESEM imaging

Conflict of Interest

The authors declare no conflict of interest.

Keywords: Ammonium nitrate · anti-ferromagnetic · bipyrimidine · coordination polymer · hydrothermal

[1] N. Marino, T. F. Mastropietro, D. Armentano, De G. Munno, R. P. Doyle, F. Lloret, F. M. Julve, *Dalton Trans.* **2008**, *777*, 5152–5154.
[2] N. Marino, D. Armentano, De G. Munno, F. Lloret, J. Cano, M. Julve, *Dalton Trans.* **2015**, *44*, 11040–11051.
[3] C. Gong, H. Guo, X. Zeng, H. Xu, Q. Zeng, J. Zhang, J. Xie, *Dalton Trans.* **2018**, *47*, 6917-.
[4] J.-X. Li, Z.-X. Du, J. Wang, X. Feng, *Z. Naturforsch. B.* **2019**, *74*, 839–845.
[5] J.-X. Li, Z.-X. Du, L.-L. Zhang, D.-L. Liu, Q.-Y. Pan, *Inorg. Chim. Acta.* **2020**,*512*,119890.
[6] Z.-X. Du, J.-X. Li, *Z. Naturforsch. B.* **2020**, *75*, 577–581.
[7] X.-H. Chang, X.-L. Ling, X.-M. Lu, X.-G. Yang, F.-F. Li, Y.-M. Guo, *J. Solid State Chem.* **2020**, *292*, 121694.
[8] H. Hu, J. Quan, Z. Tan, J.-H. Fu, Y.-J. Liang, J.-X. Li, *Russ. J. Gen. Chem.* **2021**,*91*,910–914.
[9] Y.-J. Liang, G. Feng, X. Zhang, J.-X. Li, Y. Jiang, *J. Struct. Chem.* **2021**, *62*, 300–308.
[10] Z. Zheng, P. Xu, Y. Jiang, Y.-J. Liang, J.-X. Li, *J. Struct. Chem.* **2021**, *62*, 292–299.
[11] J.-X. Li, Y.-H. Zhang, Z.-X. Du, X. Feng, *Inorg. Chim. Acta.* **2022**, *530*, 120697.
[12] J.-X. Li, Y.-Q. Xia, L.-M. Cheng, X. Feng, *J. Solid State Chem.* **2022**, *313*, 12327.
[13] H. N. Abdelhamid, *Appl. Organomet. Chem.* **2021**,*35*, .

[14] H. M. El-Bery, H. N. Abdelhamid, *J.Environ.Chem.Eng.* **2021**,*9*, 1057021.
[15] S. A. Al Kiey, H. N. Abdelhamid, *J. Energy Storage* **2022**,*55*, 105449.
[16] S. Roy, S. Choubey, S. Khan, K. Bhar, J. Ribas, B. K. Ghosh, *J. Mol. Struct.* **2014**,*1061*, 54–60.
[17] M. K. Jahn, E. Méndez, K. P. R. Nair, P. D. Godfrey, D. McNaughton, E. Patricia, F. J. Basterretxea, E. J. Cocinero, J.-U. Grabow, *Phys. Chem. Chem. Phys.* **2015**, *17*, 19726–19734.
[18] L. R. D'souza, N. N. Harmalkar, S. S. Harmalkar, S. B. Tayade, S. N. Dhuri, *ACS Omega.* **2022**, *7*, 5698–5712.
[19] C. Villa-Pérez, J. F. Cadavid-Vargas, G. E. Camí, F. Giannini, M. E. C. Villalba, G. Echeverria, I. C. Ortega, G. C. Valencia-Uribe, S. B. Etcheverry, D. B. Soria, *Inorg. Chim. Acta* **2016**, *447*, 127–133.
[20] J. Brunzelle, A. Fitch, Y. Wang, S. F. Pavkovic, *Acta Crystallogr. Sect. C* **1996**, *52*, 2984–2987.
[21] D. Armentano, G. De Munno, F. Lloret, M. Julve, *Inorg. Chem.* **1999**, *38*, 3744–3747.
[22] G. De Munno, T. Poerio, M. Julve, F. Lloret, G. Viau, *New J. Chem.* **1998**, *22*, 299–305.
[23] S. R. Marshall, C. D. Incarvito, J. L. Manson, A. L. Rheingold, J. S. Miller, *Inorg. Chem.* **2000**, *39*, 1969–1973.
[24] F. S. Delgado, J. Sanchiz, C. Ruiz-Pérez, F. Lloret, M. Julve, *CrystEngComm.* **2003**, *5*, 280–284.
[25] R. Seetharaj, P. V. Vandana, P. Arya, S. Mathew, *Arab. J. Chem.* **2019**, *12*, 295–315.
[26] G. De Munno, M. Julve, F. Lloret, J. Faus, A. Caneschi, *J. Chem. Soc., Dalton Trans.* **1994**, 1175–1183.
[27] O. Fabelo, J. Pasán, F. Lloret, M. Julve, C. Ruiz-Pérez, *Inorg. Chem.* **2008**, *47*, 3568–3576.
[28] P. Albores, E. Rentschler, *Dalton Trans.* **2013**, *42*, 9621–9627.
[29] G. De Munno, T. Poerio, G. Viau, M. Julve, F. Lloret, Y. Journaux, E. Riviere, *Chem. Commun.* **1996**, *2*, 2587–2588.
[30] G. Brewer, E. Sinn, *Inorg. Chem.* **1985**, *24*, 4580–4584.
[31] J. S. Varela, H. Sakiyama, J. Cano, E. Colacio, *Dalton Trans.* **2007**, 249–256.
[32] L. Tang, H.-H. Wang, Y.-H. Fu, Y.-T. Wang, J.-J. Wang, X.Y. Hou, *RSC Adv.* **2019**, *9*, 38902–38911.https://doi.org/10.1039/c9ra07737e
[33] D. I. Alexandropoulos, B. S. Dolinar, H. Xie, K. R. Vignesh, K. R. Dunbar, *Chem. Commun.* **2019**, *55*, 12356–12359.
[34] S. Chaturvedi, P. N. Dave, *J. Energ. Mater.* **2013**, *31*, 1–26.
[35] Y. Wang, X. Song, F. Li, *ACS Omega.* **2019**,*4*, 214–225.
[36] J. C. Oxley, J. L. Smith, E. Rogers, M. Yu, *Thermochim. Acta.* **2002**, *384*, 23–45.
[37] K. Shiota, H. Matsunaga, A. Miyake, *J. Therm. Anal. Calorim.* **2015**, *121*, 281–286.
[38] K. B. Larionov, I. V. Mishakov, A. A. Gromov, A. V. Zenkov, *J. Phys.* **2018**, *1128*, 012065.
[39] L. R. D'souza, S. K. Gaonkar, S. S. Harmalkar, P. A. Asogekar, I. Furtado, S. N. Dhuri, *ChemistrySelect.* **2021**,*6*, 1328–1336.
[40] L. R. D'souza, S. S. Harmalkar, N. N. Harmalkar, R. J. Butcher, A. S. Pal, P. A. Asogekar, S. N. Dhuri, *J. Mol. Struct.* **2022**, *1257*, 132572.
[41] M. Thommes, K. Kaneko, A. V. Neimark, J. P. Olivier, F. R. Reinoso, J. Rouquerol, K. S. W. Sing, *Pure Appl. Chem.* **2015**, *87*, 1051–1069.
[42] M. B. Yahia, Y. B. Torkia, S. Knani, M. A. Hachicha, M. Khalfaoui, A. B. Lamine, *Adsorption Scienc & Technology* **2013**, *31*, 341–357.
[43] K. A. Cychosz, M. Thommes, *Engineering.* **2018**, *4*, 559–566.
[44] R. Bardestani, G. S. Patience, S. Kaliaguine, *Can. J. Chem. Eng.* **2019**, *97*, 2781–2791.
[45] M. Nasrollahzadeh, M. Atarod, M. Sajjadi, S. M. Sajadi, Z. Issaabadi, *Interface Sci. Technol.*, Academic Press, United States, **2019**, p.199.
[46] R. Liu, Y. Meng, D. Gu, B. Tu, D. Zhao, *Stud.Surf. Sci. Catal.*, Elsevier BV, Netherlands, **2007**, p. 1721.
[47] M. F. De Lange, T. J. H. Vlugt, J. Gascon, F. Kapteijn, *Microporous Mesoporous Mater.* **2014**, *200*, 199–215.
[48] G. M. Sheldrick, *Acta Crystallogr. Sect. C* **2015**, *71*, 3–8.

Submitted: August 2, 2022
Accepted: November 18, 2022